molecular pharmaceutics

pubs.acs.org/molecularpharmaceutics

Article

Cytosolic Delivery of Small Protein Scaffolds Enables Efficient Inhibition of Ras and Myc

Alexander Chan, Hejia Henry Wang, Rebecca M. Haley, Cindy Song, David Gonzalez-Martinez, Lukasz Bugaj, Michael J. Mitchell,* and Andrew Tsourkas*

Cite This: https://doi.org/10.1021/acs.molpharmaceut.1c00798

Read Online

ACCESS | Metrics & More | Article Recommendations | Supporting Information

ABSTRACT: The ability to deliver small protein scaffolds intracellularly could enable the targeting and inhibition of many therapeutic targets that are not currently amenable to inhibition with small-molecule drugs. Here, we report the engineering of small protein scaffolds with anionic polypeptides (ApPs) to promote electrostatic interactions with positively charged nonviral lipid-based delivery systems. Proteins fused with ApPs are either complexed with off-the-shelf cationic lipids or encapsulated within ionizable lipid nanoparticles for highly efficient cytosolic delivery (up to 90%). The delivery of protein inhibitors is used to inhibit two common proto-oncogenes, Ras and Myc, in two cancer cell lines. This report demonstrates the feasibility of combining minimally engineered small protein scaffolds with tractable nanocarriers to inhibit intracellular proteins that are generally considered "undruggable" with current small molecule drugs and biologics.

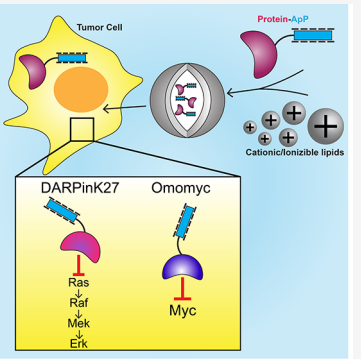

KEYWORDS: *intracellular delivery, protein delivery, undruggable proteome, Ras, Myc, lipid nanoparticles*

INTRODUCTION

The development of therapeutics that are capable of targeting the so-called "undruggable proteome" remains a challenge.[1−3] While most small molecule drugs can readily cross the cell membrane, their pharmacological effects require docking within deep functional or allosteric binding pockets, which are difficult to identify in several important therapeutic targets.[4,5] Conversely, protein biologics including antibodies, antibody fragments, and antibody mimetics display exquisite specificity and can easily inhibit these same targets by relying on expansive protein−protein interaction (PPI) interfaces; however, most proteins cannot pass through the plasma membrane to become cytosolically available, limiting their use to surface-bound receptors or secreted antigens.

Interest in cytosolically accessible protein-based therapeutics has spurred development of many delivery technologies in recent years. In one approach, potent Ras-inhibiting antibodies were engineered with integrin-binding moieties as well as an endosomal escape motif to enhance cellular internalization and cytosolic access.[6,7] Another common strategy for shuttling proteins into cells involves functionalization with cell-penetrating peptides.[8−10] Carrier-based platforms for protein delivery including virus-like particles, polymers, and inorganic nanoparticles have also been reported.[11−13] Boronic acid or guanidinium-enriched cationic polymers, which enhance native protein−polymer interactions, have also been successfully developed for the cytosolic delivery of proteins.[14,15] Our group recently developed a system whereby off-the-shelf immunoglobulin G (IgG) antibodies are labeled with anionic polypeptides (ApPs) and then complexed to cationic lipids for efficient cytosolic delivery and inhibition of intracellular targets.[16] This approach takes advantage of technology developed for nucleic acid delivery to enable the cytosolic delivery of proteins and has been used to deliver gene-editing enzymes.[17,18] Briefly, full-length antibodies were conjugated to a photoreactive antibody binding domain (pAbBD) fused with polyaspartic acid or polyglutamic acid residues. These highly negatively charged IgG−$(ApP)_2$ conjugates were then mixed with cationic lipids (e.g., Lipofectamine 2000) and delivered intracellularly by simple incubation with cells. This method enabled up to 90% cytosolic delivery efficiency of IgGs. Complexed antibodies were able to escape the endosome and retain affinity for intracellular targets. The Lipofectamine-delivered antibodies were able to inhibit MRP1 drug efflux pumps, sensitizing tumor cells to chemotherapy, and block nuclear localization of the NFκB transcription factor.

While full-length antibodies are advantageous owing to their high affinity and ability to bind virtually any protein target, their large size (>150 kDa) and multidomain structures with interchain disulfide bonds generally require expression in

Received: October 19, 2021
Revised: February 18, 2022
Accepted: February 18, 2022

eukaryotic systems, which can lead to high production costs. In a research setting, this can hinder the ability to rapidly test a multitude of hypotheses. These challenges have driven the development of inexpensive, stable, and monomeric protein binders. For example, camelid IgGs containing only heavy chains have garnered intense interest as human antibody alternatives due to the lack of interchain disulfide bonds.[19] The variable domains isolated from such heavy chain-only antibodies, known as nanobodies, are only 15 kDa and are expressed as single-domain molecules. Nanobodies have been screened against a myriad of antigens including cytoskeletal components,[20] cancer-related proteins,[21−23] and even the SARS-CoV-2 spike protein.[24,25] Beyond antibody fragments, other small protein binder formats have been developed or engineered. Such biomacromolecules include Designed Ankyrin Repeat Proteins (DARPins), which recognize antigens with the same affinity as antibodies but are much more robust than multidomain IgGs.[26] Screening of DARPin combinatorial libraries has yielded low picomolar to nanomolar binders of several therapeutic targets including VEGF[27] and KRAS.[28] Importantly, DARPin binders can be expressed at high yields in low-cost *E. coli* cultures and typically lack disulfide bonds, improving thermo-chemical stability.

The favorable biophysical properties of small protein binders can offer many benefits over full-length antibodies for biomedical applications. To capitalize on the scalability and therapeutic potential of small protein scaffolds, we applied our ApP/cationic lipid strategy to such proteins. First, we cloned and purified various small binding proteins, including a nanobody (aGFPnb), DARPin (DARPinK27), and Omomyc miniprotein, with or without the highly negatively charged ApP tags fused to the C-terminus. These anionic binders can be either complexed with off-the-shelf cationic lipids or encapsulated within ionizable lipid nanoparticles (LNPs). In either case, our method permits highly efficient membrane penetration while maintaining inhibitory function against "undruggable" oncogenic proteins. To demonstrate intracellular activity, we show that the delivery of an anti-Ras DARPin inhibits canonical MAPK signaling in both nonsmall cell lung cancer (NSCLC) and colorectal cancer cells. Second, we show that the delivery of the Myc-inhibiting miniprotein, Omomyc, blocks Myc-responsive transcription in A549 NSCLC cells. Both Ras and Myc have been identified as important oncologic targets that have generally proven to be intractable for traditional small molecule drug discovery. In this report, we present an efficient and versatile method of delivering various small protein binders intracellularly. Our method enables high delivery efficiency using both cationic lipids and ionizable LNPs (up to 90%) and functional targeting of two of the most common proto-oncogenic pathways.

MATERIALS AND METHODS

Protein Cloning and Expression. For all cloning, DNA encoding recombinant proteins were synthesized by Integrated DNA Technologies (Coralville, IA). All proteins were expressed and purified in either previously described STEPL[61] or PBSL[62] one-step purification/ligation systems. Purified proteins were concentrated using Amicon Ultra centrifugal filter units with 10 kDa MWCO (MilliporeSigma; Burlington, MA) and stored at −80 °C for further use. Protein concentration was determined by the BCA assay (ThermoFisher; Waltham, MA). Constructs were cloned with flexible GS-rich linkers between binding protein, ApP, and s11 sequences.

To generate DARPinK27-s11 and DARPinK27n3-s11 plasmids, gene blocks were inserted into the pRSET backbone containing C-terminal s11-SpyTag (pPBSL) between NdeI and XhoI with Infusion cloning (Takara Bio USA; Mountain View, CA). For ApP-tagged DARPinK27 or DARPinK27n3, inserts were purified by double digestion at NdeI/XhoI followed by gel extraction. Genes were ligated into PBSL-based plasmids with the C-terminal D30-s11-SpyTag sequence. All plasmids were confirmed by Sanger sequencing. For PBSL purification of DARPinK27 constructs, plasmids were transformed into T7 Express competent *E. coli* (New England Biolabs; Ipswich, MA). Bacterial cultures were grown for 20−22 h at 37 °C in LB-based autoinduction media (Formedium; Hunstanton, UK) with 0.6% glycerol and 100 μg/mL ampicillin. All DARPinK27 constructs except for DARPinK27n3-s11 were later transferred to pSTEPL by double digestion of PBSL plasmids at NdeI/AgeI, removal of the insert by gel extraction, and reinsertion into a pSTEPL vector using T4 ligase. The final purified protein is the same between the two systems, but we found that DARPinK27 proteins expressed well in STEPL and did not necessitate PBSL.

For aGFPnb-s11, aGFPnb-D30-s11, Omomyc-s11, and Omomyc-E30-s11, expression plasmids were cloned as outlined above into the PBSL vectors, transformed into T7 Express cells, and grown in autoinduction media with 0.6% glycerol and 100 μg/mL ampicillin. Both aGFPnb-s11 and Omomyc-s11 cultures were grown for 24 h at 37 °C, while aGFPnb-D30-s11 and Omomyc-E30-s11 cultures were grown at 25 °C for 48 h and 37 °C for 16−20 h, respectively. Protein sequences, corresponding molecular weights, and theoretical isoelectric points (pI) are listed in Table S1.

Cell Culture. A549 cells were obtained from our own stock and maintained in complete DMEM media containing 10% FBS and 1% penicillin/streptomycin. A549 splitGFP(1-10) cells, which we previously described,[16] were maintained in complete DMEM supplemented with 2 μg/mL puromycin (Takara Bio). HCT116 cells were gifted by Michael Farwell and grown in McCoy 5A media with 10% FBS and 1% penicillin/streptomycin. Both HCT116 splitGFP(1-10) and HCT116 splitGFP(1-10)/RBD-mCherry cells were grown in the same media supplemented with 2 μg/mL puromycin. All cells were maintained in a 5% CO_2, 37 °C humidified incubator.

Generating HCT116 splitGFP(1-10) Cells. Concentrated VSV-G pseudotyped lentivirus containing CMV-driven splitGFP(1-10)-IRES-PuroR was generously gifted by Philip Zoltick. HCT116 cells were incubated overnight with different volumes of lentivirus in complete McCoy 5A medium with 8 μg/mL Polybrene. The following day, media was replaced with complete McCoy 5A without Polybrene, and cells were grown to confluence for an additional 5 days. Cells expressing splitGFP(1-10) were selected with media containing 2 μg/mL puromycin. To confirm splitGFP(1-10) expression, transduced cells were pelleted, lysed in cell lysis buffer (Cell Signaling Technology 9803; Danvers, MA) with added protease inhibitor (Cell Signaling Technology 5871), and centrifuged to remove debris. Clarified lysates were incubated with purified recombinant pAbBD-s11 in TNG buffer (100 mM Tris-HCl, 150 mM NaCl, 10% v/v glycerol, pH 7.4) for at least 1 h at 37 °C, and reconstituted GFP fluorescence was analyzed on a BioTek Synergy H1 (Winooski, VT) microplate reader in

https://doi.org/10.1021/acs.molpharmaceut.1c00798
Mol. Pharmaceutics XXXX, XXX, XXX−XXX

black-bottom 96-well plates ($\lambda_{excitation}/\lambda_{emission}$ = 488 nm/530 nm). Polyclonal HCT116 splitGFP(1-10) cells with high GFP complementation were frozen for further use.

Generating HCT116 splitGFP(1-10)/RBD-mCherry Dual Reporter Cells. The live Ras fluorescent sensor (RBD-mCherry) was cloned by inserting $cRaf_{51-220}$ into a pHR lentivirus backbone plasmid already containing mCherry using NEB Builder HiFi DNA assembly master mix (New England Biolabs). Lentivirus carrying the RBD-mCherry construct was produced in HEK293T cells according to standard protocols. For stable expression of RBD-mCherry, HCT116 splitGFP(1-10) cells were incubated with lentivirus overnight. Following a media exchange, cells were grown to confluency and frozen for further use.

Ionizable Lipid Synthesis. The ionizable lipid used was synthesized by reacting epoxide-terminated alkyl chains (Avanti Polar Lipids; Alabaster, AL) with polyamine cores (Enamine; Monmouth Jct, NJ) using Michael addition chemistry, as previously described.[63] Components were combined with a 7-fold excess of alkyl chains and mixed with a magnetic stir bar for 48 h at 80 °C. The crude product was then transferred to a Rotavapor R-300 (BUCHI; Newark, DE) for solvent evaporation, and the lipids were suspended in ethanol for use in formulation.

LNP Formulation. To synthesize LNPs, an aqueous phase containing DARPinK27 protein and an ethanol phase containing lipid and cholesterol components were mixed using a microfluidic device as previously described.[63] The aqueous phase was prepared using PBS shifted to pH 5. To prepare the ethanol phase, ionizable lipid, 1,2-dioleoyl-3-trimethylammonium-propane (DOTAP), 1,2-distearoyl-*sn*-glycero-3-phosphocholine (DSPC) (Avanti Polar Lipids), lipid-anchored polyethylene glycol (PEG), and cholesterol (Sigma; St. Louis, MO) components were combined. Pump 33 DS syringe pumps (Harvard Apparatus; Holliston, MA) were used to mix the ethanol and aqueous phases at a 3:1 ratio in a microfluidic device. After mixing, LNPs were dialyzed against 1× PBS for 1 h to remove ethanol.

LNP Characterization. The hydrodynamic diameter (Z_{avg}) of LNP:DARPinK7 is 207 ± 3 nm as determined by dynamic light scattering. To determine protein concentration, a micro-BCA protein assay kit (ThermoFisher) was used. LNPs were diluted in PBS with 2% SDS, as per manufacturer instructions, to accommodate the presence of lipids in the sample. BCA working reagent was added to each sample, and samples were incubated for 2 h at 37 °C in a sonicating bath to allow for quantification of encapsulated as well as free or surface-anchored protein. Samples were plated in triplicate in 96-well plates, and the resulting absorbance was measured on a plate reader alongside a standard curve of DARPinK27 used to quantify protein concentration.

LNP Encapsulation Efficiency. To determine encapsulation efficiency of LNPs, DARPinK27-D30-s11 was first labeled with a C-terminal carboxytetramethyl rhodamine (TAMRA) using STEPL. Fluorescently labeled protein was formulated in LNPs as described above and separated from free protein by size exclusion chromatography in a column packed with 22 cm of Sepharose CL-4B resin. Fractions were mixed with equal volumes of 0.1% Triton-X in black-bottom 96-well plates, and TAMRA-fluorescence was measured in a plate reader. Peaks were integrated in GraphPad to determine the area under the curve (AUC).

Protein Isoelectric Point. DARPinK27-s11 and DARPinK27-D30-s11 in PBS were diluted 1:20−1:10 in water, which was pH adjusted with 1 M HCl. Zeta potentials of the samples were measured on a Malvern Zetasizer instrument at various pH values. The theoretical charges of proteins under different conditions were calculated using the ProtParam module from the Bio.SeqUtils package.

Binding Assay. DARPinK27n3-s11, DARPinK27-s11, and DARPinK27-D30-s11 were first labeled with a C-terminal biotin using PBSL (DARPinK27n3-s11) or STEPL (DARPinK27-s11 and DARPinK27-D30-s11). Biotinylated DARPins were serially diluted and coated onto Pierce streptavidin coated plates overnight at 4 °C. Wells were then incubated with 5 μg/mL recombinant human KRAS (Abcam 156968) at RT for 1 h. To detect DARPin-bound KRAS, wells were incubated with an anti-Ras rabbit primary antibody (Cell Signaling Technology 3339, 1:1000 dilution) followed by an HRP-conjugated anti-rabbit antibody (Invitrogen 31460, 1:4000 dilution). Both antibody incubations were performed at RT for 1 h. Binding was detected using the QuantaRed substrate kit (ThermoFisher 15159) according to the manufacturer's instructions. Wells were washed three times with 0.05% PBST between each incubation step, and all proteins and antibodies were diluted in SuperBlock T20 blocking buffer. Binding curves were fit with a 4-parameter sigmoidal model in GraphPad following background subtraction (wells without DARPin).

Protein Delivery. In a typical delivery assay, either 35 000 cells were seeded overnight in a 48-well plate format or 600 000 cells were seeded in a 6-well format. For Lipofectamine delivery in 48-well plates, 2 μL of Lipofectamine 2000 (Invitrogen; Waltham, MA) was mixed with 8 μL of Opti-MEM Reduced Serum Medium (ThermoFisher), and protein was diluted to 10 μM in 10 μL of Opti-MEM. The diluted Lipofectamine and protein solutions were mixed by pipetting 5−10 times. Proteins were incubated for 15 min at room temperature to promote complexation. Then, Lipofectamine/protein complexes were added to cells in 180 μL of antibiotic-free media so that the total protein concentration per well was 500 nM. For 6-well format delivery, all reagents except Lipofectamine were scaled 10-fold (Lipofectamine scaled 7.5-fold). For LNP delivery, indicated amounts of LNP:protein formulations were added directly to each well. Cells were incubated with proteins for 6 h at 37 °C before flow cytometry analysis and either 6 or 8 h for Western blot analysis.

Fluorescent Microscopy. To visualize splitGFP complementation in live cells, proteins were first delivered for 5.5 h into splitGFP(1-10) cells via Lipofectamine or LNPs. Then, Hoechst (50 μg/mL) was added to the cells to stain nuclei for an additional 30 min before replacing media with live cell imaging solution (ThermoFisher A14291D). Fluorescent images were acquired on an Olympus IX 81, motorized inverted microscope at 20× magnification. Images were equalized using ImageJ software.

Time-Course Confocal Microscopy. For live-cell visualization of Ras inhibition dynamics, HCT116 splitGFP(1-10)/RBD-mCherry cells were first seeded overnight in a 96-well glass plate. The following day, cells were treated with 5 μL of either LNP:K27-D30-s11 or LNP:K27n3-D30-s11. Fluorescent images were acquired on a Nikon Ti2E spinning disk confocal microscope (Melville, NY) at 40× magnification every 10 min for a total of 18 h. Temperature and CO_2 concentrations were maintained at 37 °C and 5%, respectively, using an Okolab environmental chamber (Ambridge, PA).

https://doi.org/10.1021/acs.molpharmaceut.1c00798
Mol. Pharmaceutics XXXX, XXX, XXX−XXX

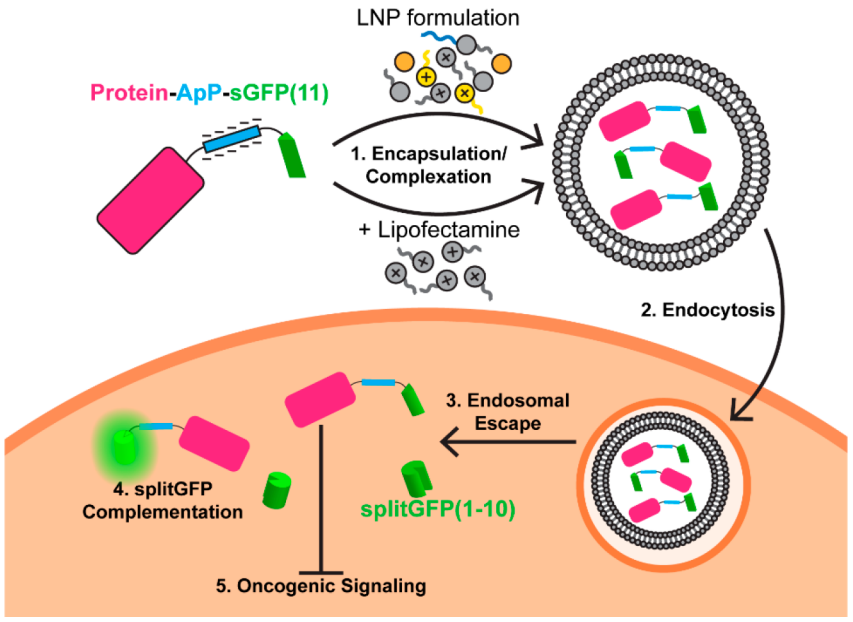

Figure 1. Schematic of cytosolic protein delivery targeting oncogenic pathways. (1) Proteins tagged with anionic polypeptides (ApPs) are encapsulated in lipid nanoparticles (LNPs) or mixed with Lipofectamine. (2) Complexed/encapsulated proteins are incubated with cells and cross the membrane. (3) Proteins escape the endosome into the cytosolic compartment. (4) The splitGFP(11) tag was appended to deliver proteins complemented with splitGFP(1-10) fragment in cells for fluorescent detection. (5) Cytosolically delivered therapeutic proteins inhibit oncogenic signaling pathways by binding intracellular targets.

Images were equalized and analyzed with ImageJ software. Individual cells were annotated and segmented into cytosolic and membrane compartments using ROI tools, and membrane localization was calculated with the equation below. Calculated membrane-to-cytosol values greater than 1.5 were considered membrane localized.

$$\frac{\text{mean intensity}_{\text{membrane}} - \text{background}}{\text{mean intensity}_{\text{cytosol}} - \text{background}}$$

Flow Cytometry. Following protein delivery in A549 splitGFP(1-10) or HCT116 splitGFP(1-10) in a 48-well plate, cells were washed once with cold PBS, detached with 0.25% trypsin, and pelleted in a 4 °C table-top centrifuge at 600*g*. Cell pellets were resuspended in flow buffer (PBS, 1% w/v BSA, 1 mM EDTA) and analyzed on a BD Accuri C6 analyzer (BD Biosciences; Franklin Lakes, NJ). At least 8000 total events were collected. Data were analyzed with BD Accuri CFlow 6 Software. Representative flow histograms were generated in FlowJo v10 (BD Biosciences). For Lipofectamine-delivered proteins, a negative control sample of 500 nM Lipofectamine-delivered pAbBD-s11 was also added.

DARPinK27 Delivery and Western Blotting. First, DARPinK27 proteins were delivered in 6-well plates for either 6 h in A549 cells or 8 h in HCT116 cells. As a positive control, cells were treated with 100 nM MEK inhibitor Trametinib for 1 h. Following delivery, cells were lysed in the plate using cell lysis buffer (Cell Signaling Technology 9803) with added protease/phosphatase inhibitor (Cell Signaling Technology 5872S) and centrifuged at 15 000*g*. Approximately 30 μg of protein was boiled in the LiCor loading buffer (LiCor 928-40004; Lincoln, NE), resolved on a NuPAGE, 4−12% Bis-Tris gel (ThermoFisher), and transferred onto a PVDF membrane for 1 h at 20 V. Membranes were blotted with mouse anti-pErk 1/2 (1:2000 dilution, Cell Signaling Technology 9106S) and rabbit anti-Erk 1/2 (1:2000 dilution, Cell Signaling Technology 9102S) primary antibodies. Membranes were then incubated with goat antirabbit 680RD (LiCor 925-68071) and donkey antimouse 800CW (LiCor 925-32212) IR-functionalized secondary antibodies (1:15 000 dilution). Imaging was performed on a LiCor Odyssey system with the fluorescent intensity in each channel set to 7. Relative protein abundance was quantitated by densitometry using ImageJ with pErk/Erk bands normalized to α-tubulin loading control (Cell Signaling Technology 2144S).

Omomyc Delivery and Luciferase Assay. Two plasmids, one encoding mouse Myc and another encoding luciferase downstream from a Myc response element were kindly provided by Kirk Wangensteen. For transient transfection, 400 000 A549 cells were seeded overnight in 6-well plates. The following day, media was replaced with 1.5 mL of antibiotic-free media. Cells were cotransfected with 1.25 μg each of the Myc overexpression and Myc reporter plasmids using Lipofectamine 3000 and P3000 reagents according to the manufacturer's instructions. After 8 h of transfection, cells were reseeded into white-bottom 96-well plates (17 500 cells/well) and allowed to adhere overnight. The following day, either 500 nM Omomyc-s11 or Omomyc-E30-s11 was delivered to cells with or without 1 μL of Lipofectamine 2000 and incubated for 4 h. After protein delivery, wells were aspirated; fresh media was added, and cells were incubated for an additional 20 h. To assay for luciferase activity, Steady-Glo reagent (Promega) was added to wells and luminescence was recorded on a microplate reader.

LDH Cytotoxicity Assay. HCT116 cells were plated overnight in 96-well plates (20 000 cells/well). The following day, media was replaced with 100 μL of antibiotic-free media with serial dilutions of LNP:K27-D30-s11, and cells were incubated for an additional 8 h. Cytotoxicity was measured using a lactate dehydrogenase (LDH) detection kit according to the manufacturer's instructions (Dojindo Molecular

https://doi.org/10.1021/acs.molpharmaceut.1c00798
Mol. Pharmaceutics XXXX, XXX, XXX−XXX

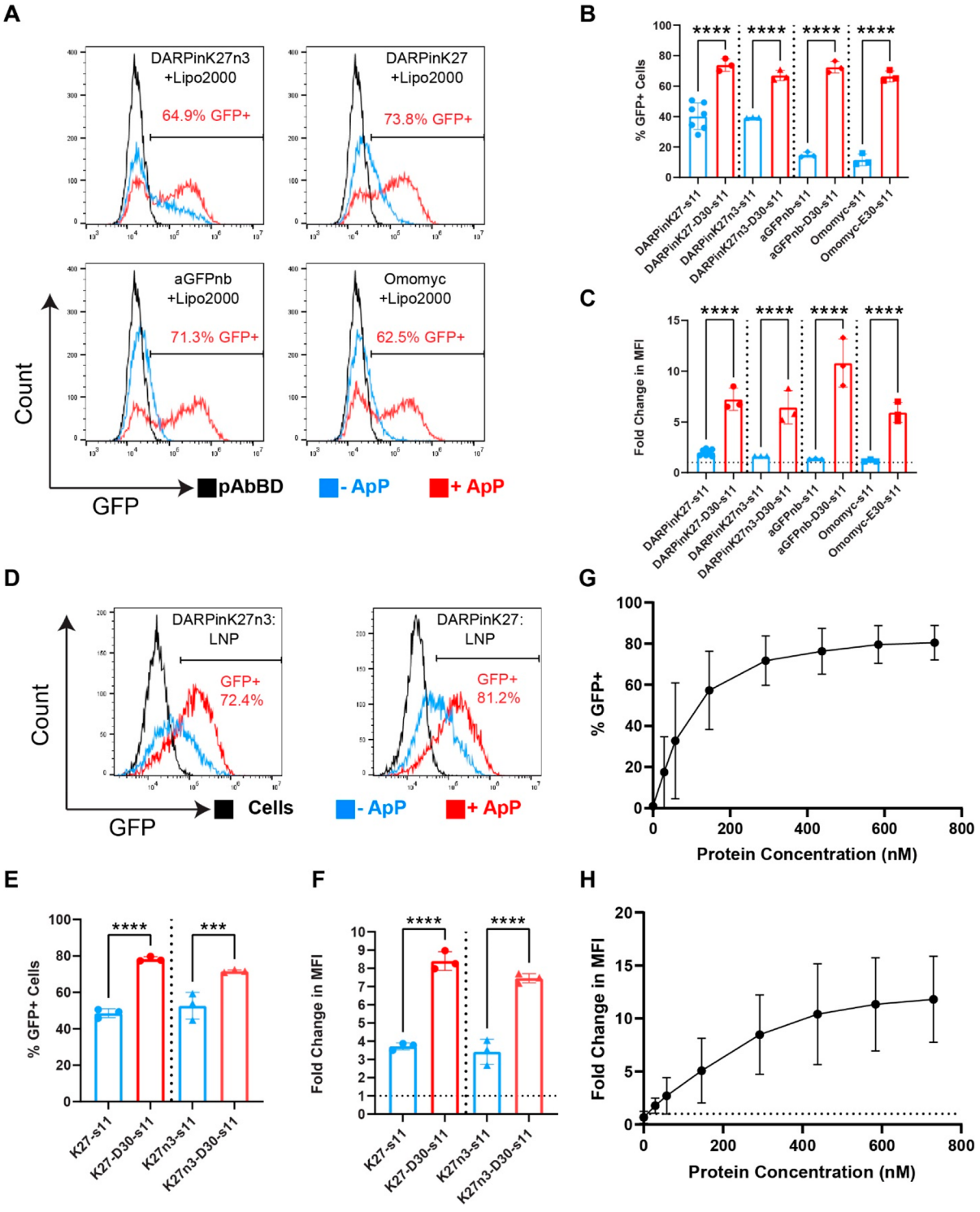

Figure 2. Cytosolic delivery of multiple protein scaffolds in cancer cells. (A) Representative flow cytometry plots of four different proteins with or without ApP tags delivered with Lipofectamine 2000. In total, 500 nM null DARPinK27n3, active DARPinK27, anti-GFP nanobody (aGFPnb), or Omomyc miniprotein were complexed with 2 μL of Lipofectamine 2000 and incubated with A549 cells stably expressing the splitGFP(1-10) fragment. After 6 h of delivery, cells were analyzed for splitGFP fluorescence by flow cytometry. (B, C) Quantification of splitGFP+ A549 cells and fold-change in median fluorescence detected following 6 h of delivery. DARPinK27-s11 was delivered at N = 7, and all other proteins were delivered at N = 3. The dotted line represents median fluorescence of 1. (D) Representative flow cytometry plots of DARPinK27n3 and DARPinK27 with or without ApP tags delivered with LNPs. In total, 10 μL of LNP/protein was delivered in HCT116 stably expressing the splitGFP(1-10) fragment. (E, F) Quantification of GFP+ HCT116 cells and fold-change in median fluorescence detected following 6 h of delivery. Proteins were delivered at N = 3. (G, H) Delivery efficiency of LNP/DARPinK27 is shown as the percent splitGFP+ cells and as fold-change in median fluorescence intensity as a function of measured protein concentration. For all flow data, blue traces/bars indicate proteins without ApP tag, while red traces/bars indicate proteins with D30 or E30 tags. The dotted line represents median fluorescence of 1. Data were analyzed by an ordinary one-way ANOVA followed by posthoc t tests with Bonferroni correction (***p < 0.001, ****p < 0.0001). Data are mean ± standard deviation. See also Figure S1.

https://doi.org/10.1021/acs.molpharmaceut.1c00798
Mol. Pharmaceutics XXXX, XXX, XXX−XXX

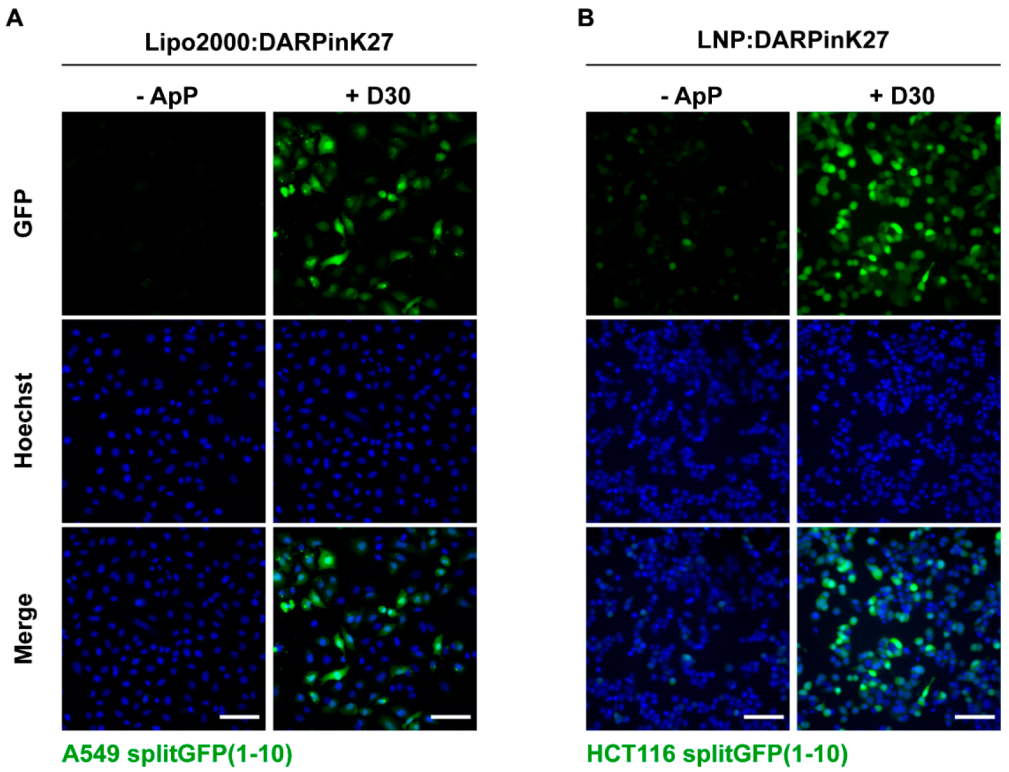

Figure 3. Fluorescent imaging of splitGFP-complemented DARPinK27 in cancer cell lines. (A) In total, 500 nM DARPinK27 with or without a D30 tag was delivered in A549 splitGFP(1-10) cells with 2 μL of Lipofectamine 2000. Fluorescence microscopy was performed 6 h after delivery. (B) To HCT116 splitGFP(1-10) cells, 10 μL of LNP:DARPinK27 with or without a D30 tag was delivered, and fluorescence microscopy was performed 6 h after delivery. Cells were also stained with Hoechst nuclear stain 30 min prior to imaging. Scale bar = 100 μm.

Technologies CK12; Rockville, MD) and normalized to both live and dead controls.

Statistical Analysis. Statistical analyses were performed with GraphPad Prism v8/v9 software or R v.4.1.1. Pairwise tests with Bonferroni or nonparametric Dunn's correction were applied as appropriate. Statistical significance was defined at α = 0.05. Multiple batches of proteins and LNPs were used throughout the study.

RESULTS

Multiple Small Protein Scaffolds Are Delivered by ApP Fusion. To determine the efficiency of intracellular delivery for various small protein scaffolds, we employed a splitGFP complementation assay whereby two nonfluorescing GFP fragments only reconstitute fluorescence when both are present and associate in the cytosolic compartment.[29] The larger of the two GFP fragments, splitGFP(1-10), which contains 10 β-strands of GFP was expressed in two cell lines: the nonsmall cell lung cancer line, A549, and the colorectal cancer cell line, HCT116. The smaller GFP fragment, i.e., the 11th GFP β-strand (denoted here as s11), was fused at the C-terminal end of the various protein scaffold-ApP fusion proteins. Three types of protein scaffolds were evaluated: DARPins, nanobodies, and the mini-protein Omomyc. To facilitate cellular uptake and endosomal−lysosomal escape of these fusion proteins, they were either complexed with off-the-shelf Lipofectamine 2000 reagent or encapsulated in LNPs. Following protein delivery, splitGFP complementation in the cytosol was detected by flow cytometry allowing for the stringent detection of intracellular protein delivery. Because splitGFP(1-10) is expressed only in the cytosol, this reporter system ensures that any protein cargo entrapped within the endosomal−lysosomal system does not result in a false-positive fluorescent signal (Figure 1).

In A549 nonsmall cell lung cancer (NSCLC) cells, the complexation of Lipofectamine 2000 with Ras-inhibiting DARPinK27, null DARPinK27n3, Omomyc miniprotein, and a GFP-binding nanobody led to significantly higher delivery efficiency when these proteins were fused with ApPs, compared with constructs that did not possess an ApP (Figure 2A−C). We used ApPs that were composed of 30 aspartic acid residues, D30 (DARPin and nanobody), or 30 glutamic acid residues, E30 (Omomyc), as we previously showed this to be an optimal ApP length for pAbBD. At 500 nM protein, all four ApP-fused constructs achieved >65% delivery efficiency when complexed with Lipofectamine 2000. DARPinK27-D30 achieved the highest delivery efficiency with 73.9 ± 4.1% of cells displaying GFP fluorescence relative to the negative control. In contrast, proteins without ApPs crossed cell membranes at much lower rates when complexed with Lipofectamine 2000, likely due to their weaker electrostatic interactions. Control DARPinK27 was delivered intracellularly at an efficiency of ∼40%, while the efficiency of intracellular delivery with control aGFPnb and Omomyc was less than 15% and 12%, respectively. In addition to the percentage of GFP-positive cells, median fluorescence intensity (MFI) was dramatically higher with protein scaffold-ApP fusions, indicating that a higher amount of protein was also delivered per cell. The MFI for ApP-fused proteins increased by up to 10-fold relative to the cell-only control in the case of aGFPnb-D30, whereas all scaffolds lacking ApPs only showed up to a 2-fold increase in MFI.

https://doi.org/10.1021/acs.molpharmaceut.1c00798
Mol. Pharmaceutics XXXX, XXX, XXX−XXX

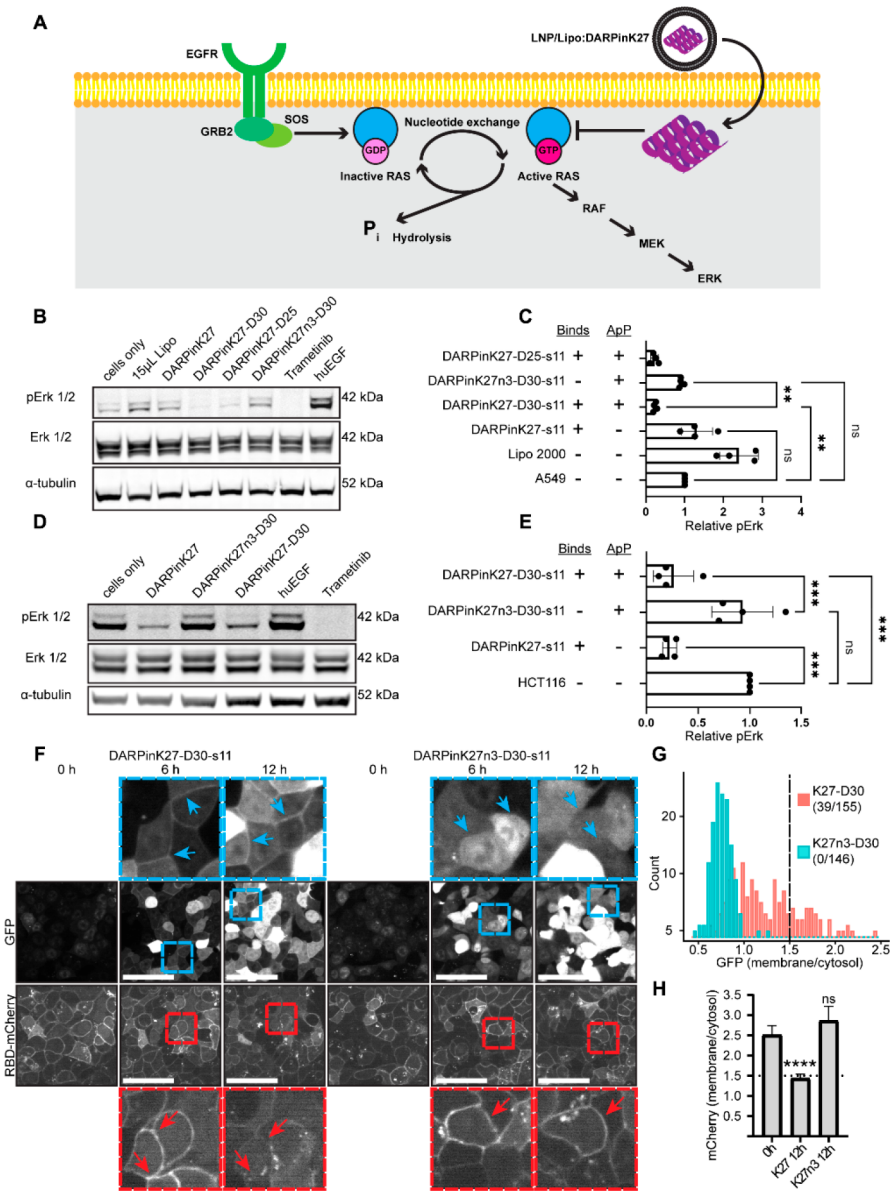

Figure 4. Inhibition of the canonical MAPK pathway. (A) Mechanism of MAPK inhibition by protein delivery. Cytosolically delivered DARPinK27 inhibits Ras kinase activity by blocking nucleotide exchange, sequestering Ras to its inactive GDP-bound form. (B, C) Active and null DARPinK27 were delivered into A549 cells at 500 nM with 15 μL of Lipofectamine 2000 in 6-well plates. Cell lysates were collected at 6 h and blotted for phosphorylated and total Erk. A representative blot is shown, and densitometry was performed on replicates (N = 4) (D, E) Active and null DARPinK27 encapsulated in LNPs were delivered into HCT116 cells at 100 μL in 6-well plates. Cell lysates were collected at 8 h and blotted for phosphorylated and total Erk. A representative blot is shown, and densitometry was performed on replicates (N = 4). All phospho-Erk signals were normalized to total Erk and loading control bands in cell-only controls. (F) Time-lapse microscopy images were taken of HCT116 splitGFP(1-10)/RBD-mCherry cells treated with either LNP:DARPinK27-D30 or LNP:DARPinK27n3-D30. Blue and red squares indicate magnified GFP and mCherry regions of interest, respectively, and arrows point to either localization or the absence of fluorescence at cell membranes. (G) Histograms of the GFP membrane/cytosol signal in dual-reporter cells 6 h after delivery and the number of cells with membrane-localized signal. (H) Amount of RBD-mCherry localization in dual-reporter cells following a 12 h delivery. The numbers of annotated cells are 92, 117, and 116 for 0 h, K27 12 h, and K27n3 12 h groups, respectively. Western blot data were analyzed by ordinary one-way ANOVA followed by posthoc unpaired t tests with Bonferroni correction, and mCherry localization was analyzed using a Kruskal–Wallis test with Dunn's correction (ns = no significance, $^{**}p < 0.01$, $^{***}p < 0.001$, $^{****}p < 0.0001$). Scale bar = 50 μm. For densitometry, data are mean ± standard deviation. For mCherry localization, data are median with 95% CI. See also Figures S3 and S5.

In HCT116 colorectal cancer cells, we initially found poor cytosolic protein delivery with Lipofectamine 2000 (Figure S1). To overcome this limitation, we chose instead to use ionizable LNPs to deliver the protein scaffolds. LNPs have been used extensively to transfect cells with nucleic acids including mRNA and siRNA[30] and offer the advantage of being amenable to *in vivo* delivery.[31,32] Ionizable LNPs encapsulate our protein scaffold-ApP fusions on the basis of the same electrostatic interaction mechanism as Lipofectamine 2000. Using an LNP formulation that incorporates a previously described ionizable lipid,[33] we were able to efficiently deliver DARPinK27 fused with a D30 ApP over a wide range of concentrations (Figure 2D–H) with minimal cytotoxicity (Figure S2). These properties suggest that ionizable LNPs are

https://doi.org/10.1021/acs.molpharmaceut.1c00798
Mol. Pharmaceutics XXXX, XXX, XXX−XXX

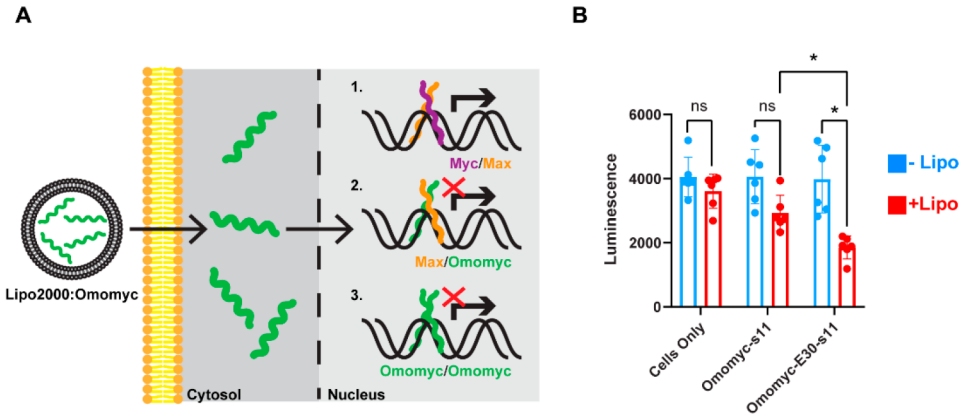

Figure 5. Inhibition of Myc-dependent transcription via cytosolic delivery of Omomyc. (A) Intracellularly delivered Omomyc miniprotein enters the nucleus to inhibit Myc activity. (1) Endogenous Myc/Max heterodimers bind to consensus promoter sequences to activate gene expression. Omomyc binds to Myc promoter regions either as heterodimer with Max (2) or as a homodimer (3). Competition at promoter regions with Myc/Max dimers block transcription of Myc target genes. (B) A549 cells were cotransfected with 1.25 μg each of a mouse Myc expression vector and a Myc-controlled luciferase reporter. Cells were then treated with 500 nM Omomyc with or without E30 ApP complexed with Lipofectamine 2000. Luciferase activity was measured 24 h after treatment with Omomyc to determine Myc transcriptional activity. For each condition, $N = 6$. Unpaired t tests were performed with Bonferroni correction for multiple comparisons (ns = no significance, $*p < 0.05$). Data are mean ± standard deviation. See also Figure S4.

excellent candidates for cytosolic protein delivery. LNP-encapsulated DARPinK27-D30 was delivered into HCT116 cells with an average efficiency of 78.2 ± 1.3% compared to 48.5 ± 2.4% without ApP (Figure 2E). Similarly, we saw an 8.4-fold change in GFP MFI for DARPinK27-D30 compared to a 3.7-fold-change for DARPinK27 without ApP (Figure 2F). Cytosolic delivery was markedly more efficient at lower total protein concentrations when using LNPs compared to Lipofectamine reagent. We achieved close to a saturating GFP signal in HCT116 GFP(1-10) cells at DARPinK27-D30 concentrations of just ∼150 nM, and a peak delivery efficiency of up to 90% at 500 nM protein (Figure 2G). In comparison, we previously showed that with Lipofectamine protein concentrations of ∼500 nM were required to approach saturating GFP signals.[16]

Protein delivery with LNPs led to a 16-fold increase in GFP MFI at around 400 nM protein (Figure 2H). Representative fluorescent microscopy images of A549 and HCT116 cells transfected with DARPinK27 using Lipofectamine or LNPs clearly indicate enhanced internalization of small protein scaffolds following fusion to ApP tags (Figure 3A,B).

Intracellularly Delivered DARPinK27 Inhibits Canonical Ras Signaling Pathway. Of the over 500 known cancer-related genes, HRAS, NRAS, and KRAS isoforms are the most frequently mutated proto-oncogenes with KRAS mutants being most prevalent. Ras family mutations are present in over 97% pancreatic cancers, 52% of colorectal cancers, and 32% of lung adenocarcinomas.[5] Ras plays a central role in multiple downstream effector pathways. The most well-known of these is the canonical RAF-MEK-ERK (MAPK) pathway, which is implicated in melanomas and NSCLC. Despite more than 30 years of research, small molecule drugs have only been developed against the $KRAS^{G12C}$ mutant, which does not account for the majority of Ras activating mutations.[34,35] To more broadly target this oncogenic pathway, we cloned and expressed recombinant DARPinK27, a pan-RAS binder that blocks the conversion of inactive GDP-bound RAS to its active GTP-bound state[36] (Figure 4A). DARPinK27 is a low nanomolar inhibitor with K_D = 4 nM but is unable to cross the plasma membrane on its own, so studies of DARPinK27 have relied on inefficient transfection and genetic expression in tumor cells.[36,37] The fusion of DARPinK27 with a D30 ApP allowed us to intracellularly deliver DARPinK27 into Ras mutant cell lines. To demonstrate that the delivered DARPinK27 was functional in the cytosol, we treated A549 and HCT116 cells with Lipofectamine-complexed or LNP-encapsulated DARPinK27, respectively, and evaluated Erk phosphorylation (pErk) to detect Ras kinase activity inhibition. After 6 h of treatment, Western blotting of A549 lysates revealed substantially lower pErk/Erk ratios in cells treated with DARPinK27-ApPs compared with untreated cells and cells treated with DARPinK27 without ApPs or Lipofectamine alone (Figure 4B). There was >75% reduction in pErk/Erk in A549 cells treated with DARPinK27-D25 or DARPinK27-D30 (Figure 4C). There was no significant change in pErk levels when A549 cells were treated either with DARPinK27 without ApPs, which we showed could not enter cells, or with a nonbinding variant, DARPinK27n3-D30.

As with A549 cells, we saw a dramatic reduction of the pErk/Erk ratio in HCT116 colorectal cancer cells treated with LNP:DAPRinK27-D30 (Figure 4D). After 8 h of treatment, pErk levels were reduced to 26 ± 19% compared to cell-only controls (Figure 4E). Again, null LNP:DARPin27n3-D30 did not affect canonical Ras signaling, as the protein contains three alanine mutations that abrogate DARPin-Ras interactions. Interestingly, a reduction of the pErk/Erk ratio was also observed with LNP:DARPinK27 (without ApP). Ras signaling inhibition was also found to be dose dependent and required LNP delivery, as free protein did not reduce Erk phosphorylation at any tested concentration (Figure S3A,B).

To investigate DARPin localization and inhibition dynamics, we engineered HCT116 splitGFP(1-10) cells with a Ras sensor comprising the cRaf-derived Ras-binding domain[38] fused to mCherry red fluorescent protein (RBD-mCherry). The RBD-mCherry sensor binds to membrane-bound GTP-Ras but not to GDP-Ras, providing a real-time method to track Ras inhibition by cytosolically delivered DARPins. Time course confocal microscopy of HCT116 dual-reporter cells treated with LNP:DARPinK27-D30-s11 showed clear recruitment of the GFP signal to the inner leaflet by 6 h (Figure 4F,G).

https://doi.org/10.1021/acs.molpharmaceut.1c00798
Mol. Pharmaceutics XXXX, XXX, XXX−XXX

Additionally, RBD-mCherry, which was initially localized to the membrane, trafficked to the cytosol by 12 h postdelivery (Figure 4H). Dual-reporter cells treated with control LNP:DARPinK27n3-D30-s11 displayed diffuse GFP fluorescence and no trafficking of RBD-mCherry to the cytosol.

Intracellularly Delivered Omomyc Blocks Myc-Dependent Transcription. We next sought to inhibit another common proto-oncogene, Myc, a key mediator of cellular growth processes. Myc dysregulation has been implicated in tumor aggressiveness and metastasis in many cancer types including triple-negative breast cancer, prostate cancer, and lung cancers.[39,40] While progress has recently been made in the development of small molecule Myc inhibitors, no small molecule inhibitors have yet to progress to clinical trials.[41,42] To target Myc-dependent activity, we delivered the dominant-negative version, Omomyc.[43] Omomyc inhibits Myc-family transcription factors by forming both nonfunctional, DNA-binding Omomyc/Omomyc homodimers, and Omomyc/Myc or Omomyc/MAX heterodimers.[44,45] Thus, Omomyc works by sequestering both available Myc and MAX molecules and consensus enhancer binding sites to block Myc-dependent gene expression (Figure 5A).

We first cotransfected A549 cells with a mouse Myc overexpression plasmid and a reporter plasmid encoding luciferase downstream of tandem E-box sequences. Then, recombinant Omomyc or Omomyc-E30 was complexed with Lipofectamine 2000 and delivered. There were no significant changes in luminescence between untreated cells and cells treated with either Omomyc-s11 or Omomyc-E30-s11 alone at 500 nM protein (Figure 5B). To validate that this poor transcription inhibition was due to poor internalization, we confirmed that neither free Omomyc-s11 nor Omomyc-E30-s11 could cross A549 cell membranes. Following 6 h of incubation with either protein, we did not observe splitGFP fluorescence with flow cytometry at free protein concentrations up to 5 μM (Figure S4). These data suggest that free Omomyc exhibits poor cell penetrability, contrary to recent findings.[46] However, when delivered with Lipofectamine, Omomyc-E30-s11 significantly decreased luminescence by 54%, whereas Omomyc-s11 showed a modest but nonsignificant decrease in luminescence. Thus, we demonstrate that Omomyc-ApP fusions proteins complexed with cationic lipids can block Myc activity.

■ DISCUSSION

Methods that can enable efficient intracellular protein delivery offer promising and novel therapeutic modalities. While there have been multiple diverse examples of protein delivery into cells, many of these strategies suffer from low delivery efficiency, complicated chemical syntheses, or utilization of materials that are not readily translatable for use *in vivo*.[47] Expanding on our previous work delivering full-length antibodies, we show that multiple small protein scaffolds can be delivered into the cytosol at high efficiency with a minimal polyanionic tag. Our 30aa ApPs enable efficient delivery and inhibition with smaller tags compared to reported supercharged GFP (240aa)[18] or Prothymosin alpha (111aa).[17] However, a direct comparison of our method is difficult owing to the amplified readout of these Cre-recombinase-based reporter systems. We further show that two inhibitory molecules, Omomyc and DARPinK27, retain functionality within the cytosol following complexation with either Lipofectamine or LNPs. Delivery of low molecular weight antibody mimics vastly enhances the biologics landscape, offering low-cost, scalable alternatives to full-length antibodies for intracellular targeted therapy and biomedical research applications. As scaffolds such as nanobodies, DARPins, and miniproteins develop clinically, we view their use as complementary to full-length IgGs. Further, this work may be adapted to deliver proteins other than inhibitors, including transcription factors or subunit antigens to antigen-presenting cells.

Excitingly, we showed excellent delivery of DARPinK27 in HCT116 cells using ionizable LNPs. Whereas Lipofectamine 2000 failed to deliver the protein in this cell line (Figure S1), ionizable LNPs delivered DARPinK27-ApP fusion proteins intracellularly with >80% efficiency at protein concentrations less than 200 nM. Several FDA-approved siRNA/mRNA-based therapies have ignited interest in LNPs as delivery vehicles. These first-in-class drugs include Patisiran for the treatment of polyneuropathy in people with hereditary transthyretin-mediated amyloidosis[48] and the Moderna and Pfizer/BioNTech mRNA vaccines for SARS-CoV-2.[49,50] However, more research is needed to systematically optimize protein encapsulation and cytosolic delivery. In support of this, we calculated an encapsulation efficiency of 27% for our initial LNP formulation (Figure S5), which may be improved through such optimization efforts. Parameters including protein/lipid ratio, choice of ionizable lipid, excipient proportions, and mixing conditions should be tuned for optimal *in vitro* and *in vivo* delivery. Furthermore, LNPs can be decorated with antibodies to target specific cell populations.[51,52] Hence, the versatility of LNPs supports further investigation of customized ionizable lipid formulations for protein delivery and can facilitate the transition away from Lipofectamine or purely cationic lipid products, which are less likely to be clinically viable as delivery agents due to their inherent toxicity. Additionally, the encapsulation of recombinant protein over nucleic acids may be advantageous, as RNA-based drugs are prone to degradation both during synthesis and following administration, necessitating chemical modifications to enhance nuclease resistance and improve their pharmacokinetic properties.[53]

Interestingly, we saw Ras inhibition with LNP:DAPRinK27 (without ApPs) in HCT116 cells, which was not observed with Lipofectamine-delivered DARPinK27 in A549 cells. To explain this, we first note that LNPs, which are typically used for nucleic acid delivery, have a high encapsulation efficiency of negatively charged cargo. The analysis of the DARPinK27 amino acid sequence (https://web.expasy.org/compute_pi/) indicates a slightly negative charge under mildly acidic conditions, which we confirmed by measuring the zeta potential of DARPinK27 under different pH conditions (Figure S6). Furthermore, ionizable lipids with a pK_a between 5 and 6 are known to promote efficient endosomal escape via pH-dependent interactions with endosomal membranes.[54,55] Indeed, we had observed strong recruitment of reconstituted splitGFP to the plasma membrane (Figure S7), indicating efficient endosomal escape of DARPin. We also noticed fewer fluorescent puncta following intracellular protein delivery with LNPs in HCT116 cells compared to intracellular protein delivery with Lipofectamine in A549 cells, suggesting higher levels of cytosolically available DARPinK27. Coupled with the high affinity of DARPinK27 for Ras, we reason that even low amounts of delivered DARPinK27 could still block Ras signaling in HCT116. Finally, we found that fusion of the

https://doi.org/10.1021/acs.molpharmaceut.1c00798
Mol. Pharmaceutics XXXX, XXX, XXX−XXX

ApP tag did not decrease the affinity of DARPinK27 toward KRAS (Figure S8).

In a second functionality study, we delivered Omomyc, a miniprotein inhibitor of Myc-family transcription factors. Omomyc was chosen because it is the most well-studied protein inhibitor of the Myc proto-oncogene. In our study, we saw substantial but incomplete inhibition of Myc-dependent transcription in A549 cells. This could be because Myc is only boosted by E-box sequences through preferential but not absolute specificity and may bind at all available promoters.[56,57] To overcome this, other Myc-inhibiting miniproteins may be explored for ApP tagging and intracellular delivery. Recently, two such proteins, dubbed MEF[58] and Mad,[59] have surfaced with the latter exhibiting greater inhibition of Myc-mediated transcription than Omomyc. In control studies, we observed that free Omomyc and Omomyc-E30 exhibited no inhibitory effect and negligible cytosolic delivery despite reports of Omomyc possessing intrinsic cell-penetrating behavior. This could potentially be explained by the high concentration of Omomyc used in prior studies (up to 12.8 μM)[46] compared with those used here (500 nM). Finally, free Omomyc suffers from poor pharmacokinetic properties *in vivo*, which may limit its usefulness in the clinic.[60] In order to protect Omomyc from degradation and rapid clearance and to modulate its biodistribution, LNPs are potentially well-suited for *in vivo* delivery. Notably, we found that Omomyc is challenging to directly encapsulate in the same LNP formulation used for DARPin. Omomyc is a long and dimeric protein compared to DARPin, which is rigid, compact, and monomeric. Additionally, Omomyc contains a highly basic N-terminal DNA-binding region. These properties may destabilize Omomyc within current LNP formulations even with the addition of an ApP. More optimization is necessary to screen ionizable lipids, which can efficiently pack and stabilize Omomyc within the LNP core. For these reasons, we have omitted this formulation from the current work.

In conclusion, we show that appending minimal polyanionic tags to small protein scaffolds enables efficient cytosolic delivery into mammalian cells by cationic or ionizable lipid nanocarriers. Fusion of either D30 or E30 ApP tags onto nanobody, DARPin, or Myc-derived miniprotein scaffolds enabled cytosolic delivery between 66% and 74% efficiency using off-the-shelf Lipofectamine, whereas free proteins had no intrinsic cell-penetrating properties (Figure S9). In cells that are not susceptible to Lipofectamine-mediated transfection, we formulated LNPs, which delivered ApP-tagged proteins at up to 90% efficiency on the basis of splitGFP complementation assays. Delivered DARPinK27 blocked the canonical Ras signaling pathway by 75%, and Omomyc reduced Myc-dependent activity by >50%. Our strategy is amenable to multiple classes of small protein scaffolds of varying structural composition from the basic helix−loop−helix leucine zipper domain of Omomyc to the ankyrin repeat motifs of DARPin. When the engineered proteins were combined with off-the-shelf cationic lipids and state-of-the-art ionizable LNPs, the therapeutic potential of the antibody mimetics for targeting intracellular targets is greatly expanded and offers an opportunity to target the undruggable proteome.

Significance. Small protein scaffolds have garnered growing interest as therapeutic platforms. They are relatively inexpensive to produce and can be screened against nearly any protein target, offering highly specific binding and neutralization ability. However, many promising therapeutic targets remain inaccessible to protein-based inhibitors due to their intracellular localization, as biomacromolecules generally cannot cross the plasma membrane. For example, two key oncogenic drivers, Ras, mutated in up to 30% of tumors, and Myc, which is also frequently amplified in cancer, remain elusive clinical targets. The development of delivery agents to ferry small protein binders into cells would greatly expand the druggable proteome and increase the repertoire of therapeutic modalities in the clinic. To address this need, we developed a method to efficiently deliver small-protein binders cytosolically and demonstrate functional inhibition of both Ras and Myc. We further demonstrate the feasibility of using LNPs, currently employed for RNA-based therapies, to deliver our engineered inhibitors, increasing the chances of successfully translating our method for *in vivo* applications.

■ ASSOCIATED CONTENT

Supporting Information

The Supporting Information is available free of charge at https://pubs.acs.org/doi/10.1021/acs.molpharmaceut.1c00798.

Flow cytometric analysis of the DARPinK27-D30-s11 delivery in HCT116 splitGFP(1-10) cells; LNP cytotoxicity in HCT116 cells; dose response of pErk 1/2 to LNP-delivered DARPinK27-D30 or free DARPinK27; flow cytometric analysis of free Omomyc into A549 splitGFP(1-10) cells; encapsulation efficiency of DARPinK27-D30 in LNPs; isoelectric point of DARPinK27 and DARPinK27-D30; fluorescence microscopy analysis of reconstituted splitGFP in HCT116 splitGFP (1-10) cells following the delivery of DARPinK27-D30; binding affinity of DARPinK27 and DARPinK27-D30; flow cytometric analysis of intracellular protein delivery without the use of cationic lipids; table with protein sequences, molecular weights, and theoretical PI (PDF)

■ AUTHOR INFORMATION

Corresponding Authors

Andrew Tsourkas − *Department of Bioengineering, University of Pennsylvania, Philadelphia, Pennsylvania 19104, United States; Abramson Cancer Center, Perelman School of Medicine and Institute for Immunology, Perelman School of Medicine, University of Pennsylvania, Philadelphia, Pennsylvania 19104, United States;* orcid.org/0000-0001-7758-1753; Email: atsourk@seas.upenn.edu

Michael J. Mitchell − *Department of Bioengineering, University of Pennsylvania, Philadelphia, Pennsylvania 19104, United States; Abramson Cancer Center, Perelman School of Medicine, Institute for Immunology, Perelman School of Medicine, Cardiovascular Institute, Perelman School of Medicine, and Institute for Regenerative Medicine, Perelman School of Medicine, University of Pennsylvania, Philadelphia, Pennsylvania 19104, United States;* orcid.org/0000-0002-3628-2244; Email: mjmitch@seas.upenn.edu

Authors

Alexander Chan − *Department of Bioengineering, University of Pennsylvania, Philadelphia, Pennsylvania 19104, United States*

https://doi.org/10.1021/acs.molpharmaceut.1c00798
Mol. Pharmaceutics XXXX, XXX, XXX−XXX

Hejia Henry Wang − *Department Biochemistry and Molecular Biophysics, University of Pennsylvania, Philadelphia, Pennsylvania 19104, United States*
Rebecca M. Haley − *Department of Bioengineering, University of Pennsylvania, Philadelphia, Pennsylvania 19104, United States*
Cindy Song − *Department of Molecular Biology and Biochemistry, Rutgers University, New Brunswick, New Jersey 08901, United States*
David Gonzalez-Martinez − *Department of Bioengineering, University of Pennsylvania, Philadelphia, Pennsylvania 19104, United States*
Lukasz Bugaj − *Department of Bioengineering, University of Pennsylvania, Philadelphia, Pennsylvania 19104, United States; Abramson Cancer Center, Perelman School of Medicine and Institute for Regenerative Medicine, Perelman School of Medicine, University of Pennsylvania, Philadelphia, Pennsylvania 19104, United States*

Complete contact information is available at: https://pubs.acs.org/10.1021/acs.molpharmaceut.1c00798

Notes

The authors declare the following competing financial interest(s): A.T. and H.H.W. have a pending patent on the technology described in this manuscript.

■ ACKNOWLEDGMENTS

We thank Michael Farwell at the University of Pennsylvania Department of Radiology for providing HCT116 cells. We also thank Philip Zoltick at the Children's Hospital of Philadelphia (CHOP) for providing splitGFP(1-10) lentivirus. We thank Kirk Wangensteen at The Perelman School of Medicine at the University of Pennsylvania for Myc expression and reporter plasmids. A.C. and R.M.H. are supported by the National Science Foundation Graduate Research Fellowship (NSF-GRFP). Work was supported by the NIH/NCI R01 CA241661, Penn Health-Tech Pilot Award, and funding from and Abramson Cancer Center (NIH/NCI P30 CA016520). M.J.M. acknowledges support from a Burroughs Wellcome Fund Career Award at the Scientific Interface (CASI) and a U.S. National Institutes of Health (NIH) Director's New Innovator Award (DP2 TR002776).

■ REFERENCES

(1) Hopkins, A. L.; Groom, C. R. The Druggable Genome. *Nat. Rev. Drug Discovery* **2002**, *1* (9), 727−730.
(2) Russ, A. P.; Lampel, S. The Druggable Genome: An Update. *Drug Discovery Today* **2005**, 1607−1610.
(3) Finan, C.; Gaulton, A.; Kruger, F. A.; Lumbers, R. T.; Shah, T.; Engmann, J.; Galver, L.; Kelley, R.; Karlsson, A.; Santos, R.; Overington, J. P.; Hingorani, A. D.; Casas, J. P. The Druggable Genome and Support for Target Identification and Validation in Drug Development. *Science Translational Medicine* **2017**, *9* (383), 1.
(4) Cox, A. D.; Fesik, S. W.; Kimmelman, A. C.; Luo, J.; Der, C. J. Drugging the Undruggable RAS: Mission Possible? *Nature Reviews Drug Discovery* **2014**, 828−851.
(5) Dang, C. v.; Reddy, E. P.; Shokat, K. M.; Soucek, L. Drugging the "undruggable" Cancer Targets. *Nature Reviews Cancer* **2017**, 502−508.
(6) Shin, S. M.; Choi, D. K.; Jung, K.; Bae, J.; Kim, J. S.; Park, S. W.; Song, K. H.; Kim, Y. S. Antibody Targeting Intracellular Oncogenic Ras Mutants Exerts Anti-Tumour Effects after Systemic Administration. *Nat. Commun.* **2017**, *8* (1), 1−14.
(7) Shin, S. M.; Kim, J. S.; Park, S. W.; Jun, S. Y.; Kweon, H. J.; Choi, D. K.; Lee, D.; Cho, Y. B.; Kim, Y. S. Direct Targeting of Oncogenic RAS Mutants with a Tumor-Specific Cytosol-Penetrating Antibody Inhibits RAS Mutant−Driven Tumor Growth. *Science Advances* **2020**, *6* (3), No. eaay2174.
(8) Zhang, J. F.; Xiong, H. L.; Cao, J. L.; Wang, S. J.; Guo, X. R.; Lin, B. Y.; Zhang, Y.; Zhao, J. H.; Wang, Y. B.; Zhang, T. Y.; Yuan, Q.; Zhang, J.; Xia, N. S. A Cell-Penetrating Whole Molecule Antibody Targeting Intracellular HBx Suppresses Hepatitis B Virus via TRIM21-Dependent Pathway. *Theranostics* **2018**, *8* (2), 549−562.
(9) Gaston, J.; Maestrali, N.; Lalle, G.; Gagnaire, M.; Masiero, A.; Dumas, B.; Dabdoubi, T.; Radosevic, K.; Berne, P.-F. Intracellular Delivery of Therapeutic Antibodies into Specific Cells Using Antibody-Peptide Fusions. *Scientific Reports* **2019**, *9*, 18688.
(10) Sauter, M.; Strieker, M.; Kleist, C.; Wischnjow, A.; Daniel, V.; Altmann, A.; Haberkorn, U.; Mier, W. Improving Antibody-Based Therapies by Chemical Engineering of Antibodies with Multimeric Cell-Penetrating Peptides for Elevated Intracellular Delivery. *J. Controlled Release* **2020**, *322*, 200−208.
(11) Fu, A.; Tang, R.; Hardie, J.; Farkas, M. E.; Rotello, V. M. Promises and Pitfalls of Intracellular Delivery of Proteins. *Bioconjugate Chemistry* **2014**, 1602−1608.
(12) Slastnikova, T. A.; Ulasov, A. v.; Rosenkranz, A. A.; Sobolev, A. S. Targeted Intracellular Delivery of Antibodies: The State of the Art. *Frontiers in Pharmacology* **2018**, *9* (OCT), 1208.
(13) Li, Y.; Li, P.; Li, R.; Xu, Q. Intracellular Antibody Delivery Mediated by Lipids, Polymers, and Inorganic Nanomaterials for Therapeutic Applications. *Advanced Therapeutics* **2020**, 2000178.
(14) Lv, J.; Fan, Q.; Wang, H.; Cheng, Y. Polymers for Cytosolic Protein Delivery. *Biomaterials* **2019**, *218*, 119358.
(15) Cheng, Y. Design of Polymers for Intracellular Protein and Peptide Delivery. *Chin. J. Chem.* **2021**, *39* (6), 1443−1449.
(16) Wang, H. H.; Tsourkas, A. Cytosolic Delivery of Inhibitory Antibodies with Cationic Lipids. *Proc. Natl. Acad. Sci. U.S.A.* **2019**, *116* (44), 22132−22139.
(17) Kim, Y. B.; Zhao, K. T.; Thompson, D. B.; Liu, D. R. An Anionic Human Protein Mediates Cationic Liposome Delivery of Genome Editing Proteins into Mammalian Cells. *Nat. Commun.* **2019**, *10*, 2905.
(18) Zuris, J. A.; Thompson, D. B.; Shu, Y.; Guilinger, J. P.; Bessen, J. L.; Hu, J. H.; Maeder, M. L.; Joung, J. K.; Chen, Z.-Y.; Liu, D. R. Cationic Lipid-Mediated Delivery of Proteins Enables Efficient Protein-Based Genome Editing in Vitro and in Vivo. *Nat. Biotechnol.* **2014**, *33* (1), 73−80.
(19) Muyldermans, S. Nanobodies: Natural Single-Domain Antibodies. *Annual Review of Biochemistry. Annual Reviews* **2013**, *82*, 775−797.
(20) Moutel, S.; Bery, N.; Bernard, V.; Keller, L.; Lemesre, E.; de Marco, A.; Ligat, L.; Rain, J. C.; Favre, G.; Olichon, A.; Perez, F. NaLi-H1: A Universal Synthetic Library of Humanized Nanobodies Providing Highly Functional Antibodies and Intrabodies. *eLife* **2016**, *5* (JULY), e16228.
(21) Buchfellner, A.; Yurlova, L.; Nüske, S.; Scholz, A. M.; Bogner, J.; Ruf, B.; Zolghadr, K.; Drexler, S. E.; Drexler, G. A.; Girst, S.; Greubel, C.; Reindl, J.; Siebenwirth, C.; Romer, T.; Friedl, A. A.; Rothbauer, U. A New Nanobody-Based Biosensor to Study Endogenous PARP1 in Vitro and in Live Human Cells. *PLoS One* **2016**, *11* (3), No. e0151041.
(22) Fenderico, N.; van Scherpenzeel, R. C.; Goldflam, M.; Proverbio, D.; Jordens, I.; Kralj, T.; Stryeck, S.; Bass, T. Z.; Hermans, G.; Ullman, C.; Aastrup, T.; Gros, P.; Maurice, M. M. Anti-LRP5/6 VHHs Promote Differentiation of Wnt-Hypersensitive Intestinal Stem Cells. *Nat. Commun.* **2019**, *10* (1), 1−13.
(23) Traenkle, B.; Emele, F.; Anton, R.; Poetz, O.; Haeussler, R. S.; Maier, J.; Kaiser, P. D.; Scholz, A. M.; Nueske, S.; Buchfellner, A.; Romer, T.; Rothbauer, U. Monitoring Interactions and Dynamics of Endogenous Beta-Catenin with Intracellular Nanobodies in Living Cells. *Mol. Cell. Proteomics* **2015**, *14* (3), 707−723.

(24) Koenig, P. A.; Das, H.; Liu, H.; Kümmerer, B. M.; Gohr, F. N.; Jenster, L. M.; Schiffelers, L. D. J.; Tesfamariam, Y. M.; Uchima, M.; Wuerth, J. D.; Gatterdam, K.; Ruetalo, N.; Christensen, M. H.; Fandrey, C. I.; Normann, S.; Tödtmann, J. M. P.; Pritzl, S.; Hanke, L.; Boos, J.; Yuan, M.; Zhu, X.; Schmid-Burgk, J. L.; Kato, H.; Schindler, M.; Wilson, I. A.; Geyer, M.; Ludwig, K. U.; Hällberg, B. M.; Wu, N. C.; Schmidt, F. I. Structure-Guided Multivalent Nanobodies Block SARS-CoV-2 Infection and Suppress Mutational Escape. *Science* **2021**, *371* (6530), 371.

(25) Xiang, Y.; Nambulli, S.; Xiao, Z.; Liu, H.; Sang, Z.; Duprex, W. P.; Schneidman-Duhovny, D.; Zhang, C.; Shi, Y. Versatile and Multivalent Nanobodies Efficiently Neutralize SARS-CoV-2. *Science* **2020**, *370* (6523), 1479−1484.

(26) Plückthun, A. Designed Ankyrin Repeat Proteins (DARPins): Binding Proteins for Research, Diagnostics, and Therapy. *Annual Review of Pharmacology and Toxicology* **2015**, *55*, 489−511.

(27) Stahl, A.; Stumpp, M. T.; Schlegel, A.; Ekawardhani, S.; Lehrling, C.; Martin, G.; Gulotti-Georgieva, M.; Villemagne, D.; Forrer, P.; Agostini, H. T.; Binz, H. K. Highly Potent VEGF-A-Antagonistic DARPins as Anti-Angiogenic Agents for Topical and Intravitreal Applications. *Angiogenesis* **2013**, *16* (1), 101−111.

(28) Bery, N.; Legg, S.; Debreczeni, J.; Breed, J.; Embrey, K.; Stubbs, C.; Kolasinska-Zwierz, P.; Barrett, N.; Marwood, R.; Watson, J.; Tart, J.; Overman, R.; Miller, A.; Phillips, C.; Minter, R.; Rabbitts, T. H. KRAS-Specific Inhibition Using a DARPin Binding to a Site in the Allosteric Lobe. *Nat. Commun.* **2019**, *10* (1), 1−11.

(29) Cabantous, S.; Terwilliger, T. C.; Waldo, G. S. Protein Tagging and Detection with Engineered Self-Assembling Fragments of Green Fluorescent Protein. *Nat. Biotechnol.* **2005**, *23* (1), 102−107.

(30) Yin, H.; Kanasty, R. L.; Eltoukhy, A. A.; Vegas, A. J.; Dorkin, J. R.; Anderson, D. G. Non-Viral Vectors for Gene-Based Therapy. *Nature Reviews Genetics* **2014**, *15* (8), 541−555.

(31) Liu, J.; Chang, J.; Jiang, Y.; Meng, X.; Sun, T.; Mao, L.; Xu, Q.; Wang, M. Fast and Efficient CRISPR/Cas9 Genome Editing In Vivo Enabled by Bioreducible Lipid and Messenger RNA Nanoparticles. *Adv. Mater.* **2019**, *31* (33), 1902575.

(32) Qiu, M.; Glass, Z.; Chen, J.; Haas, M.; Jin, X.; Zhao, X.; Rui, X.; Ye, Z.; Li, Y.; Zhang, F.; Xu, Q. Lipid Nanoparticle-Mediated Codelivery of Cas9MRNA and Single-Guide RNA Achieves Liver-Specific in Vivo Genome Editing of Angptl3. *Proc. Natl. Acad. Sci. U. S. A.* **2021**, *118* (10), e2020401118.

(33) Billingsley, M. M.; Singh, N.; Ravikumar, P.; Zhang, R.; June, C. H.; Mitchell, M. J. Ionizable Lipid Nanoparticle-Mediated MRNA Delivery for Human CAR T Cell Engineering. *Nano Lett.* **2020**, *20* (3), 1578−1589.

(34) Canon, J.; Rex, K.; Saiki, A. Y.; Mohr, C.; Cooke, K.; Bagal, D.; Gaida, K.; Holt, T.; Knutson, C. G.; Koppada, N.; Lanman, B. A.; Werner, J.; Rapaport, A. S.; San Miguel, T.; Ortiz, R.; Osgood, T.; Sun, J.-R.; Zhu, X.; McCarter, J. D.; Volak, L. P.; Houk, B. E.; Fakih, M. G.; O'Neil, B. H.; Price, T. J.; Falchook, G. S.; Desai, J.; Kuo, J.; Govindan, R.; Hong, D. S.; Ouyang, W.; Henary, H.; Arvedson, T.; Cee, V. J.; Lipford, J. R. The Clinical KRAS(G12C) Inhibitor AMG 510 Drives Anti-Tumour Immunity. *Nature* **2019**, No. 7781, 217−223.

(35) Hong, D. S.; Fakih, M. G.; Strickler, J. H.; Desai, J.; Durm, G. A.; Shapiro, G. I.; Falchook, G. S.; Price, T. J.; Sacher, A.; Denlinger, C. S.; Bang, Y.-J.; Dy, G. K.; Krauss, J. C.; Kuboki, Y.; Kuo, J. C.; Coveler, A. L.; Park, K.; Kim, T. W.; Barlesi, F.; Munster, P. N.; Ramalingam, S. S.; Burns, T. F.; Meric-Bernstam, F.; Henary, H.; Ngang, J.; Ngarmchamnanrith, G.; Kim, J.; Houk, B. E.; Canon, J.; Lipford, J. R.; Friberg, G.; Lito, P.; Govindan, R.; Li, B. T. KRASG12C Inhibition with Sotorasib in Advanced Solid Tumors. *N. Engl. J. Med.* **2020**, *383* (13), 1207−1217.

(36) Guillard, S.; Kolasinska-Zwierz, P.; Debreczeni, J.; Breed, J.; Zhang, J.; Bery, N.; Marwood, R.; Tart, J.; Overman, R.; Stocki, P.; Mistry, B.; Phillips, C.; Rabbitts, T.; Jackson, R.; Minter, R. Structural and Functional Characterization of a DARPin Which Inhibits Ras Nucleotide Exchange. *Nat. Commun.* **2017**, *8* (1), 1−11.

(37) Lim, S.; Khoo, R.; Juang, Y.-C.; Gopal, P.; Zhang, H.; Yeo, C.; Peh, K. M.; Teo, J.; Ng, S.; Henry, B.; Partridge, A. W. Exquisitely Specific Anti-KRAS Biodegraders Inform on the Cellular Prevalence of Nucleotide-Loaded States. *ACS Central Science* **2021**, *7* (2), 274−291.

(38) Bondeva, T.; Balla, A.; Várnai, P.; Balla, T. Structural Determinants of Ras-Raf Interaction Analyzed in Live Cells. *Mol. Biol. Cell* **2002**, *13* (7), 2323−2333.

(39) Dang, C. v. MYC on the Path to Cancer. *Cell. Elsevier B.V* **2012**, *149*, 22−35.

(40) Wolfer, A.; Wittner, B. S.; Irimia, D.; Flavin, R. J.; Lupien, M.; Gunawardane, R. N.; Meyer, C. A.; Lightcap, E. S.; Tamayo, P.; Mesirov, J. P.; Liu, X. S.; Shioda, T.; Toner, M.; Loda, M.; Brown, M.; Brugge, J. S.; Ramaswamy, S. MYC Regulation of a "Poor-Prognosis" Metastatic Cancer Cell State. *Proc. Natl. Acad. Sci. U.S.A.* **2010**, *107* (8), 3698−3703.

(41) Han, H.; Jain, A. D.; Truica, M. I.; Izquierdo-Ferrer, J.; Anker, J. F.; Lysy, B.; Sagar, V.; Luan, Y.; Chalmers, Z. R.; Unno, K.; Mok, H.; Vatapalli, R.; Yoo, Y. A.; Rodriguez, Y.; Kandela, I.; Parker, J. B.; Chakravarti, D.; Mishra, R. K.; Schiltz, G. E.; Abdulkadir, S. A. Small-Molecule MYC Inhibitors Suppress Tumor Growth and Enhance Immunotherapy. *Cancer Cell* **2019**, *36* (5), 483−497.E15.

(42) Madden, S. K.; de Araujo, A. D.; Gerhardt, M.; Fairlie, D. P.; Mason, J. M. Taking the Myc out of Cancer: Toward Therapeutic Strategies to Directly Inhibit c-Myc. *Molecular Cancer* **2021**, *20* (1), 1−18.

(43) Soucek, L.; Helmer-Citterich, M.; Sacco, A.; Jucker, R.; Cesareni, G.; Nasi, S. Design and Properties of a Myc Derivative That Efficiently Homodimerizes. *Oncogene* **1998**, *17* (19), 2463−2472.

(44) Jung, L. A.; Gebhardt, A.; Koelmel, W.; Ade, C. P.; Walz, S.; Kuper, J.; von Eyss, B.; Letschert, S.; Redel, C.; D'Artista, L.; Biankin, A.; Zender, L.; Sauer, M.; Wolf, E.; Evan, G.; Kisker, C.; Eilers, M. OmoMYC Blunts Promoter Invasion by Oncogenic MYC to Inhibit Gene Expression Characteristic of MYC-Dependent Tumors. *Oncogene* **2017**, *36* (14), 1911−1924.

(45) Savino, M.; Annibali, D.; Carucci, N.; Favuzzi, E.; Cole, M. D.; Evan, G. I.; Soucek, L.; Nasi, S. The Action Mechanism of the Myc Inhibitor Termed Omomyc May Give Clues on How to Target Myc for Cancer Therapy. *PLoS One* **2011**, *6* (7), No. e22284.

(46) Beaulieu, M.-E.; Jauset, T.; Massó-Vallés, D.; Martínez-Martín, S.; Rahl, P.; Maltais, L.; Zacarias-Fluck, M. F.; Casacuberta-Serra, S.; del Pozo, E. S.; Fiore, C.; Foradada, L.; Cano, V. C.; Sánchez-Hervás, M.; Guenther, M.; Sanz, E. R.; Oteo, M.; Tremblay, C.; Martín, G.; Letourneau, D.; Montagne, M.; Alonso, M. Á. M.; Whitfield, J. R.; Lavigne, P.; Soucek, L. Intrinsic Cell-Penetrating Activity Propels Omomyc from Proof of Concept to Viable Anti-MYC Therapy. *Science Translational Medicine* **2019**, *11* (484), 5012.

(47) Goswami, R.; Jeon, T.; Nagaraj, H.; Zhai, S.; Rotello, V. M. Accessing Intracellular Targets through Nanocarrier-Mediated Cytosolic Protein Delivery. *Trends Pharmacol. Sci.* **2020**, *41* (10), 743−754.

(48) Adams, D.; Gonzalez-Duarte, A.; O'Riordan, W. D.; Yang, C.-C.; Ueda, M.; Kristen, A. v.; Tournev, I.; Schmidt, H. H.; Coelho, T.; Berk, J. L.; Lin, K.-P.; Vita, G.; Attarian, S.; Planté-Bordeneuve, V.; Mezei, M. M.; Campistol, J. M.; Buades, J.; Brannagan, T. H.; Kim, B. J.; Oh, J.; Parman, Y.; Sekijima, Y.; Hawkins, P. N.; Solomon, S. D.; Polydefkis, M.; Dyck, P. J.; Gandhi, P. J.; Goyal, S.; Chen, J.; Strahs, A. L.; Nochur, S. v.; Sweetser, M. T.; Garg, P. P.; Vaishnaw, A. K.; Gollob, J. A.; Suhr, O. B. Patisiran, an RNAi Therapeutic, for Hereditary Transthyretin Amyloidosis. *N. Engl. J. Med.* **2018**, *379* (1), 11−21.

(49) Baden, L. R.; El Sahly, H. M.; Essink, B.; Kotloff, K.; Frey, S.; Novak, R.; Diemert, D.; Spector, S. A.; Rouphael, N.; Creech, C. B.; McGettigan, J.; Khetan, S.; Segall, N.; Solis, J.; Brosz, A.; Fierro, C.; Schwartz, H.; Neuzil, K.; Corey, L.; Gilbert, P.; Janes, H.; Follmann, D.; Marovich, M.; Mascola, J.; Polakowski, L.; Ledgerwood, J.; Graham, B. S.; Bennett, H.; Pajon, R.; Knightly, C.; Leav, B.; Deng, W.; Zhou, H.; Han, S.; Ivarsson, M.; Miller, J.; Zaks, T. Efficacy and

https://doi.org/10.1021/acs.molpharmaceut.1c00798
Mol. Pharmaceutics XXXX, XXX, XXX−XXX

Safety of the MRNA-1273 SARS-CoV-2 Vaccine. 10.1056/NEJMoa2035389. *N. Engl. J. Med.* **2021**, *384* (5), 403−416.
(50) Polack, F. P.; Thomas, S. J.; Kitchin, N.; Absalon, J.; Gurtman, A.; Lockhart, S.; Perez, J. L.; Marc, G. P.; Moreira, E. D.; Zerbini, C.; Bailey, R.; Swanson, K. A.; Roychoudhury, S.; Koury, K.; Li, P.; Kalina, W. v.; Cooper, D.; Frenck, Robert W.; Hammitt, L. L.; Türeci, Ö.; Nell, H.; Schaefer, A.; Ünal, S.; Tresnan, D. B.; Mather, S.; Dormitzer, P. R.; Şahin, U.; Jansen, K. U.; Gruber, W. C. Safety and Efficacy of the BNT162b2MRNA Covid-19 Vaccine. *N. Engl. J. Med.* **2020**, *383* (27), 2603−2615.
(51) Katakowski, J. A.; Mukherjee, G.; Wilner, S. E.; Maier, K. E.; Harrison, M. T.; di Lorenzo, T. P.; Levy, M.; Palliser, D. Delivery of SiRNAs to Dendritic Cells Using DEC205-Targeted Lipid Nanoparticles to Inhibit Immune Responses. *Molecular Therapy* **2016**, *24* (1), 146−155.
(52) Ramishetti, S.; Kedmi, R.; Goldsmith, M.; Leonard, F.; Sprague, A. G.; Godin, B.; Gozin, M.; Cullis, P. R.; Dykxhoorn, D. M.; Peer, D. Systemic Gene Silencing in Primary T Lymphocytes Using Targeted Lipid Nanoparticles. *ACS Nano* **2015**, *9* (7), 6706−6716.
(53) Roberts, T. C.; Langer, R.; Wood, M. J. A. Advances in Oligonucleotide Drug Delivery. *Nature Reviews Drug Discovery 2020 19:10* **2020**, *19* (10), 673−694.
(54) Hafez, I. M.; Maurer, N.; Cullis, P. R. On the Mechanism Whereby Cationic Lipids Promote Intracellular Delivery of Polynucleic Acids. *Gene Ther.* **2001**, *8* (15), 1188−1196.
(55) Hajj, K. A.; Ball, R. L.; Deluty, S. B.; Singh, S. R.; Strelkova, D.; Knapp, C. M.; Whitehead, K. A. Branched-Tail Lipid Nanoparticles Potently Deliver MRNA In Vivo Due to Enhanced Ionization at Endosomal PH. *Small* **2019**, *15* (6), 1805097.
(56) Nie, Z.; Hu, G.; Wei, G.; Cui, K.; Yamane, A.; Resch, W.; Wang, R.; Green, D. R.; Tessarollo, L.; Casellas, R.; Zhao, K.; Levens, D. C-Myc Is a Universal Amplifier of Expressed Genes in Lymphocytes and Embryonic Stem Cells. *Cell* **2012**, *151* (1), 68−79.
(57) Nie, Z.; Guo, C.; Das, S. K.; Chow, C. C.; Batchelor, E.; Simons, S. S.; Levens, D. Dissecting Transcriptional Amplification by MYC. *eLife* **2020**, *9*, e52483.
(58) Inamoto, I.; Sheoran, I.; Popa, S. C.; Hussain, M.; Shin, J. A. Combining Rational Design and Continuous Evolution on Minimalist Proteins That Target the E-Box DNA Site. *ACS Chem. Biol.* **2021**, *16* (1), 35−44.
(59) Demma, M. J.; Hohn, M. J.; Sun, A.; Mapelli, C.; Hall, B.; Walji, A.; O'Neil, J. Inhibition of Myc Transcriptional Activity by a Mini-Protein Based upon Mxd1. *FEBS Lett.* **2020**, *594* (10), 1467−1476.
(60) Demma, M. J.; Mapelli, C.; Sun, A.; Bodea, S.; Ruprecht, B.; Javaid, S.; Wiswell, D.; Muise, E.; Chen, S.; Zelina, J.; Orvieto, F.; Santoprete, A.; Altezza, S.; Tucci, F.; Escandon, E.; Hall, B.; Ray, K.; Walji, A.; O'Neil, J. Omomyc Reveals New Mechanisms To Inhibit the MYC Oncogene. *Mol. Cell. Biol.* **2019**, *39* (22), 1.
(61) Warden-Rothman, R.; Caturegli, I.; Popik, V.; Tsourkas, A. Sortase-Tag Expressed Protein Ligation: Combining Protein Purification and Site-Specific Bioconjugation into a Single Step. *Anal. Chem.* **2013**, *85* (22), 11090−11097.
(62) Wang, H. H.; Altun, B.; Nwe, K.; Tsourkas, A. Proximity-Based Sortase-Mediated Ligation. *Angew. Chem., Int. Ed.* **2017**, *56* (19), 5349−5352.
(63) Billingsley, M. M.; Singh, N.; Ravikumar, P.; Zhang, R.; June, C. H.; Mitchell, M. J. Ionizable Lipid Nanoparticle-Mediated MRNA Delivery for Human CAR T Cell Engineering. *Nano Lett.* **2020**, *20* (3), 1578−1589.

https://doi.org/10.1021/acs.molpharmaceut.1c00798
Mol. Pharmaceutics XXXX, XXX, XXX−XXX